nature geoscience

ARTICLES

PUBLISHED ONLINE: 10 OCTOBER 2010 | DOI: 10.1038/NGEO977

Complex rupture during the 12 January 2010 Haiti earthquake

G. P. Hayes[1,2]*, R. W. Briggs[1], A. Sladen[3], E. J. Fielding[4], C. Prentice[5], K. Hudnut[6], P. Mann[7], F. W. Taylor[7], A. J. Crone[1], R. Gold[1], T. Ito[3,8] and M. Simons[3]

Initially, the devastating M_w 7.0, 12 January 2010 Haiti earthquake seemed to involve straightforward accommodation of oblique relative motion between the Caribbean and North American plates along the Enriquillo–Plantain Garden fault zone. Here, we combine seismological observations, geologic field data and space geodetic measurements to show that, instead, the rupture process involved slip on multiple faults. Primary surface deformation was driven by rupture on blind thrust faults with only minor, deep, lateral slip along or near the main Enriquillo–Plantain Garden fault zone; thus the event only partially relieved centuries of accumulated left-lateral strain on a small part of the plate-boundary system. Together with the predominance of shallow off-fault thrusting, the lack of surface deformation implies that remaining shallow shear strain will be released in future surface-rupturing earthquakes on the Enriquillo–Plantain Garden fault zone, as occurred in inferred Holocene and probable historic events. We suggest that the geological signature of this earthquake—broad warping and coastal deformation rather than surface rupture along the main fault zone—will not be easily recognized by standard palaeoseismic studies. We conclude that similarly complex earthquakes in tectonic environments that accommodate both translation and convergence—such as the San Andreas fault through the Transverse Ranges of California—may be missing from the prehistoric earthquake record.

The societal impact of the 12 January 2010 Haiti earthquake (hereafter referred to as the 2010 Léogâne earthquake, after the region of principal coseismic uplift) was immense, with over 230,000 deaths and 8–14 billion dollars in damage attributed directly to the event[1]. Much of this impact was centred in the densely populated and impoverished conurbation of Port-au-Prince, the capital city of Haiti. The earthquake was an unfortunate confirmation of previous geodetic and geologic analyses[2–4] that documented the potential for large, damaging earthquakes in the region. In this study we combine seismological, geologic and geodetic data to provide a detailed characterization of the earthquake source. An integrated account of coseismic rupture helps explain how strain is accommodated along plate-boundary structures, and will be used to develop realistic seismic-hazard assessments that will guide rebuilding efforts in Haiti. The tectonic complexity of this earthquake also provides important lessons for future analyses of other transpressional tectonic regimes worldwide.

Data

Despite occurring along a well-expressed major fault system, the 2010 Léogâne earthquake is considerably more complex than preliminary seismological analyses suggested. The US Geological Survey (USGS) National Earthquake Information Center (NEIC) located this earthquake at 18.44° N, 72.57° W, at a depth of 13 km, with an origin time of 21:53:10 UTC and a moment magnitude of M_w 7.0 (http://www.earthquake.usgs.gov/earthquakes/eqinthenews/2010/us2010rja6/). The global centroid moment tensor (http://www.globalcmt.org/CMTsearch.html) solution for the event indicates shallow focus, and slip on a steeply dipping left-lateral strike-slip fault (strike $\phi = 251°$, dip $\delta = 70°$, rake $\lambda = 28°$, moment $M_0 = 4.7 \times 10^{19}$ N m). Similar parameters were obtained by body-wave moment tensor ($\phi = 246°$, $\delta = 74°$, $\lambda = 23°$, $M_0 = 4.4 \times 10^{19}$ N m) and the W-phase ($\phi = 249°$, $\delta = 74°$, $\lambda = 22°$, $M_0 = 4.4 \times 10^{19}$ N m) inversions at the USGS NEIC. The initial location and mechanism for this event suggested rupture on the Enriquillo–Plantain Garden fault zone (EPGF), a major left-lateral fault system that accommodates 7 ± 2 mm yr^{-1} of relative motion between the Caribbean plate and Gonâve microplates[3,5], part of the broader Caribbean–North America plate boundary (Fig. 1). The EPGF is the probable source of several large historic earthquakes in the region (National Oceanic and Atmospheric Administration (NOAA) National Geophysical Data Center (NGDC); http://www.ngdc.noaa.gov/hazard/hazards.shtml) including major events in November 1751 and June 1770. Both caused significant damage in Port-au-Prince; several hundred fatalities were directly attributed to the 1770 event (NOAA NGDC).

Several lines of seismological evidence show the complex nature of the 2010 Léogâne earthquake rupture. First, all moment-tensor solutions by NEIC and the global centroid moment tensor have a significant non-double couple component (as measured by the compensated linear vector dipole ratio f_{clvd}, ranging between 0.16 and 0.22 for the three solutions discussed above), indicative of a complex source composed of two or more subevents on non-parallel fault structures or in non-synchronous ruptures[6]. Second, a single-plane finite fault model (Supplementary Fig. S1) derived from teleseismic body- and surface-wave data further suggests source complexity: inversions indicate a peak slip of ~6.0 m updip and close to the hypocentre, with significant slip extending ~25–30 km west of the hypocentre and a complex pattern of lateral and thrust motion. Finally, the aftershock distribution from initial teleseismic locations, and from events located by an array of postearthquake portable instruments, are consistently

[1]US Geological Survey, Golden, Colorado 80401, USA, [2]Synergetics Inc., Fort Collins, Colorado 80524, USA, [3]California Institute of Technology, Pasadena, California 91125, USA, [4]Jet Propulsion Laboratory, California Institute of Technology, Pasadena, California 91109, USA, [5]US Geological Survey, Menlo Park, California 94025, USA, [6]US Geological Survey, Pasadena, California 91106, USA, [7]University of Texas Institute of Geophysics, Jackson School of Geosciences, University of Texas, Austin 78758, USA, [8]Nagoya University 464-8601, Japan. *e-mail: ghayes@usgs.gov.

NATURE GEOSCIENCE DOI: 10.1038/NGEO977

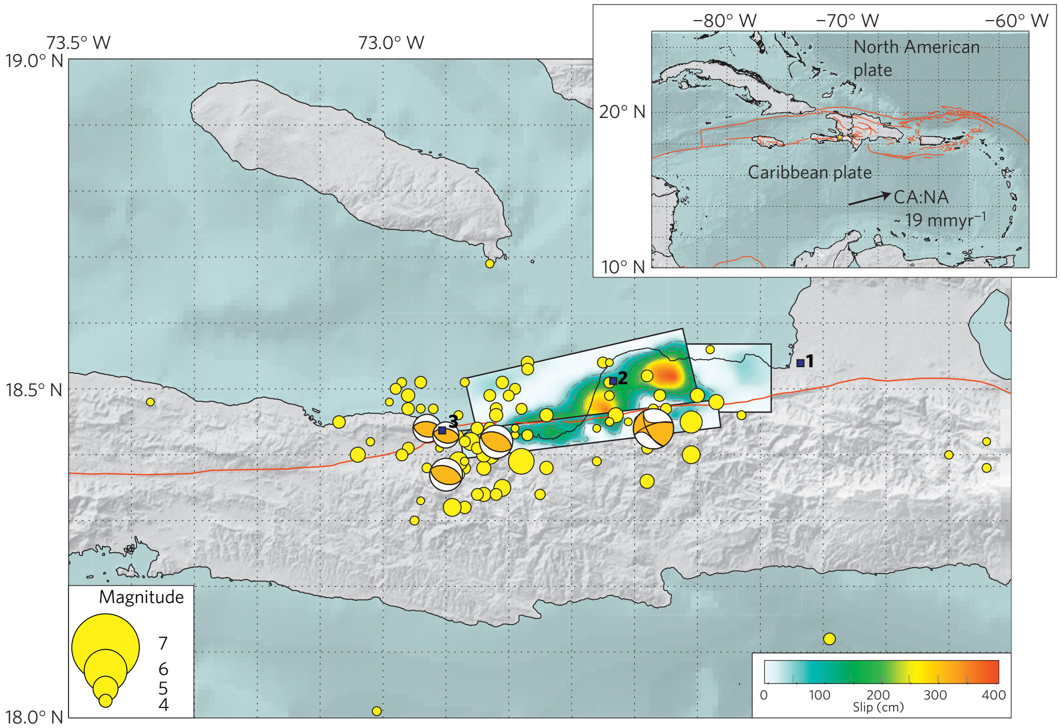

Figure 1 | Tectonic setting of the 2010 Léogâne earthquake. The inset shows the broad configuration of the Caribbean–North America plate boundary in the region of Hispaniola, with major faults (red) and the relative-plate-motion vector (arrow). The main panel shows the epicentral region of the 12 January 2010 earthquake. Aftershocks (yellow circles), sized by magnitude, and CMT solutions are shown at their NEIC locations. The surface projection of coseismic slip on each major subfault is coloured and contoured (dashed lines) by slip amplitude, at 50 cm intervals. The approximate location of the EPGF is shown in red. Numbered blue squares represent major population centres: 1 = Port-au-Prince, 2 = Léogâne, 3 = Port Royal.

offset from the main EPGF, which dips steeply to the south where observed near the epicentre[7]. Preliminary moment-tensor solutions for aftershocks[8] (Fig. 1) indicate northwest/southeast-oriented thrust motions, in contrast to the dominantly strike-slip mechanism of the mainshock. The diffuse distribution of the aftershocks, which are located primarily at the western margin of the region of significant slip identified in this study and the region of coseismic deformation imaged by interferometric synthetic aperture radar (InSAR), suggests that most of these events reflect triggered slip on minor faults that form part of a complex fault system, rather than defining the mainshock coseismic rupture zone.

The InSAR-derived surface-deformation field demonstrates that rupture was not confined to simple strike-slip on the EPGF. Instead, combinations of ascending and descending Advanced Land Observation Satellite phased-array-type L-band synthetic aperture radar (PALSAR) interferograms, which isolate the vertical (Fig. 2, main panel) and east (Fig. 2e) components of deformation, show a broad uplift pattern centred north of the EPGF. Uplift extends across the Léogâne fan delta (and presumably offshore) and a broad subsidence trough is centred on the mountains of the Massif de la Selle, with the line of zero change located several kilometres south of the inferred surface trace of the EPGF. Curiously, an approximately 12-km-wide patch of east-directed motion occurs directly north of the EPGF towards the eastern end of the rupture (Fig. 2e), which is inconsistent with simple left-lateral slip on the EPGF and a further indication of source complexity. The descending track wrapped interferogram (Supplementary Fig. S9) shows that rupture extended 40 km to the west of the hypocentre and the continuity of fringes across the EPGF indicates that no significant surface rupture occurred on the fault system.

Field observations confirm that no primary surface rupture occurred on the main EPGF; instead, the primary geologic signal is broad regions of uplift and subsidence that are particularly well expressed along the coast (Fig. 2, Supplementary Fig. S2). Elevated coral reefs along 55 km of coastline from Gressier to Port Royal record as much as 0.64 ± 0.11 m of coseismic uplift (Fig. 2a,c,d). We observed uplift primarily using microatolls of the species *Siderastrea siderea* and the genus *Diploria*, which function as natural tide recorders[9,10]. Extensive shaking-induced spreading and slumping of unconsolidated coastal deposits is superimposed on the tectonically raised coast, causing complex patterns of uplift overprinted with local subsidence (Fig. 2b,d). True tectonic subsidence of the coastline is restricted to a 3-km-long section west of Petit Goâve that was dropped by <20 cm. A comparison of uplift values from coral and beach geomorphic measurements and the vertical component of deformation derived from InSAR (Fig. 2) shows good agreement.

Joint-inversion rupture model

To integrate the seismologic, geodetic and geologic observations, we develop a detailed rupture model based on a joint inversion of InSAR, coral measurements and teleseismic body-wave data (see Methods). The preferred model requires slip on three faults to recreate the principal geodetic and seismologic features of the rupture (Fig. 3).

The broad uplift bulge north of the EPGF across the Léogâne fan delta (Fig. 2) is best fitted by a 55° N-dipping blind thrust fault (Fig. 3, fault B), called herein the Léogâne fault. Slip on the Léogâne fault accounts for the coastal uplift from Gressier to Petit Goâve and reproduces the broad subsidence trough observed in the mountains to the south. The western end of the fault is constrained by the hinge line of zero uplift in Petit Goâve identified by field geologic studies. This fault is responsible for about 80% of the moment released during the event, and the inversion predicts maximum slip of approximately 3.5 m. A south-dipping fault can also fit the observed

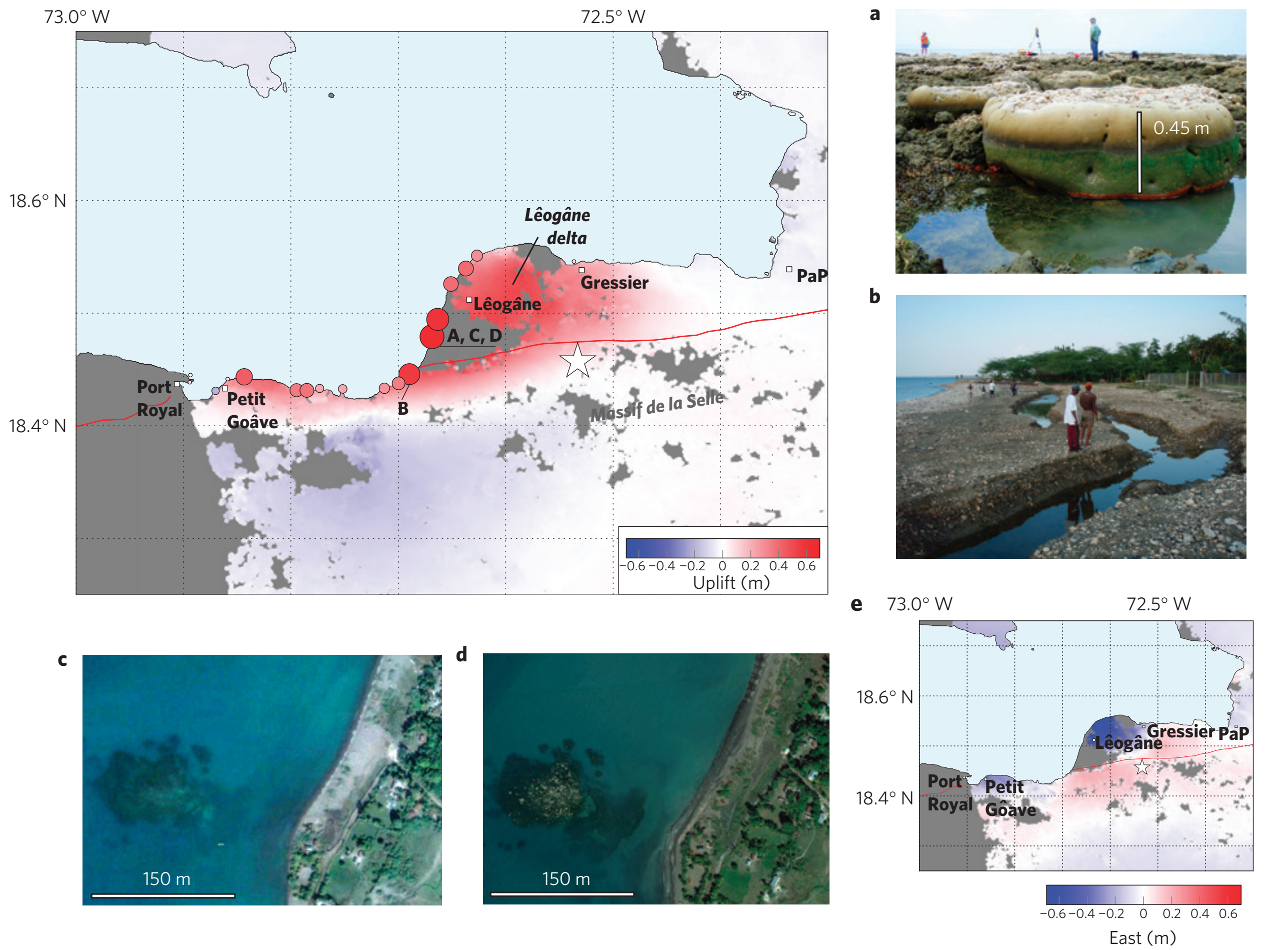

Figure 2 | Observed coastal uplift and vertical-deformation signal from InSAR. Circles denote observation points, sized and coloured by their amounts of uplift (blue denotes subsidence). The white star represents the NEIC hypocentre. Major population centres are shown with white squares (PaP = Port-au-Prince). The colour map represents the vertical component of ground motion from the sum of the ascending and descending interferograms. The approximate location of the EPGF is shown in red. **a**, *Siderastrea siderea* microatoll uplifted by 0.64 ± 0.11 m at Beloc site. Coral die-down was 0.45 m at the time of measurement. **b**, Deep fractures caused by lateral spreading along the coast at Bellevue. **c**,**d**, Images of patch reef adjacent to Beloc before the earthquake (**c**) in 2005 (Digital Globe) and after the earthquake (**d**) in January 2010 (Google). In **d** the bleached uplifted reef reflects tectonic uplift whereas extensive lateral spreading along the coast has caused localized secondary subsidence. **e**, Estimates of the east component of the ground motion from the difference of the ascending and descending interferograms.

surface-uplift pattern, but less successfully fits the broad subsidence trough south of the EPGF and the left-lateral motion identified by seismology (Supplementary Fig. S5); nor does such a model explain well the observed coseismic observations from GPS studies[11].

The Léogâne fault is geometrically consistent with the overall style of faulting in the Central Haiti fold-and-thrust belt[12]. However, a single north-dipping thrust fault does not account for the patch of east-directed movement north of the EPGF at the eastern end of the rupture, mentioned above. This small patch of surface motion, which is opposite to the long-term left-lateral displacement on the EPGF, is best modelled by a 45° south-dipping fault that has a maximum slip of approximately 1.5 m. The south-dipping geometry implies that a transfer zone exists between this fault and the blind thrust fault (the Léogâne fault), which approximately aligns with the sharp topography between the Léogâne fan delta and the mountains to the east (Fig. 1).

Seismologic data suggest that part of the rupture occurred as left-lateral slip along a steeply dipping fault (Supplementary Figs S1, S11, S12), a signal that is not apparent from geodetic data alone. The most likely source of this slip is a fault similar in orientation and strike to the 70° south-dipping EPGF (ref. 7). Because the EPGF has a complex surface expression in the rupture area[7], we model slip on a plane striking 83° that has an average orientation similar to that of the EPGF. This modelled fault has a maximum slip of approximately 2.2 m and mainly occurs at depths below 5 km. Including this fault in the inversion helps explain the steep deformation gradient (tight curvature and closely spaced InSAR fringes) near the EPGF, and also helps reproduce the non-double couple component in the event moment tensors (Supplementary Fig. S11). The limited resolution of our analysis prevents us from determining whether the EPGF, or an unmapped, subparallel and blind fault or series of faults, is the source of the deep left-lateral slip.

A puzzling geologic aspect of the 2010 Léogâne earthquake rupture is the occurrence of 2.5 km of continuous, east/west-trending, apparent tectonic fracturing and warping near Port Royal that has normal-slip offsets up to 15 cm but no lateral displacement[7]. Residents report that the cracks appeared on 12 January; however, the feature does not clearly align with breaks in the InSAR interferogram fringes, nor is the normal sense of motion clearly represented in the seismologic source or aftershock moment tensors. Because of ambiguity associated with these fractures, and the possibility that they are associated with triggered slip or an early aftershock, we do not attempt to model them as part of the mainshock rupture source here.

NATURE GEOSCIENCE DOI: 10.1038/NGEO977

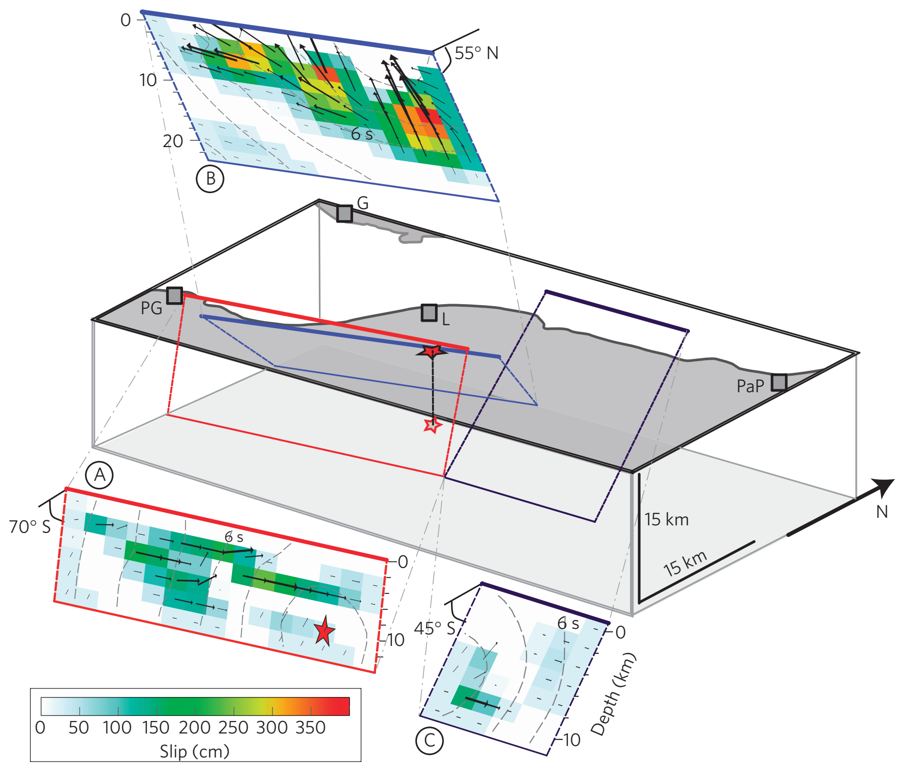

Figure 3 | Three-dimensional view of proposed fault geometry for Léogâne earthquake rupture. View to the northwest. Thick solid lines are the surface projection of each fault. Dash-dot lines link planes to cross-sectional projections of their slip distributions. Arrows represent the slip direction, scaled by amplitude, for each fault. Rupture initiates on the steep EPGF (A) at the earthquake hypocentre (star), extending to the west. The backside of the shallowly north-dipping blind thrust (Léogâne fault, B) is visible near the hypocentre and to the west. Rupture also occurs on a south-dipping structure to the east of the hypocentre (C), whose surface projection occurs north of the peninsula coastline. On each fault plane, black dashed lines are isochrons of the earthquake rupture, in 2 s increments (6 s contour labelled for reference). PaP = Port-au-Prince, L = Léogâne, PG = Petit Goâve, G = Ile de la Gonave.

Hidden earthquakes and future hazard

A primary question that arises from the observations presented here is whether any part of the 2010 Léogâne earthquake involved slip on the EPGF. The broad uplift bulge north of the EPGF (Fig. 2) and lack of surface rupture on the main fault zone imply that most, and possibly all, of the slip occurred on subsidiary faults. The InSAR-derived surface-deformation field can be adequately modelled by one or more shallow, blind thrust faults. However, information from the seismic wavefield (Supplementary Fig. S8)—in particular the occurrence of left-lateral slip on a steeply dipping structure and the complexity in the moment tensor solutions for the event (Supplementary Fig. S11)—indicate that some portion of the rupture occurred as deep lateral motion on a steeply dipping fault, perhaps the EPGF or a nearby subparallel structure, in addition to slip on thrust faults to the north. If the EPGF was involved in this rupture, then it contributed only a small amount of deep lateral slip. The primary mode of deformation on the EPGF is left-lateral slip as identified by surface geologic observations[7] and did not occur on 12 January.

Integration of the geodetic and seismologic data further demonstrates that the 2010 Léogâne earthquake relieved only limited shear strain across the broad EPGF system (Fig. 4). The relative amounts of horizontal and vertical moment release along the source faults imply along-strike (that is, horizontal) moment release of 2.71×10^{19} N m, and along-dip (that is, vertical $\div \cos\delta$) moment release of 2.86×10^{19} N m. If the EPGF has a horizontal slip rate of 7 mm yr^{-1}, it accumulates 3.15×10^{8} N m of moment per year per m^2 of fault area, using a shear modulus of 45 GPa (derived using the slip inversion subfault moment-weighted average). The total area of significant slip (both horizontal and vertical) in our model is approximately 6.9×10^{8} m^2. Using this area and annual rate, it takes roughly 125 years to accumulate the amount of horizontal moment released in this earthquake. Partitioning this total area by the same ratio with which moment release is resolved into horizontal and vertical components, this time is approximately 250 years. This estimate is approximately equal to the time that has elapsed since the most recent large earthquakes along this fault zone (1751 and 1770), and implies that, at least over the 25×10 km patch of deep fault area where lateral slip was focused, strain accumulated since the most recent set of events has been completely relaxed. However, over the shallow section of the faults where slip either did not occur or was predominantly vertical, significant accumulated strain remains (Fig. 4). This accumulated shear strain is equivalent to about 2–3 m of slip, over an area of approximately 30 km × 5 km. If released in one earthquake, this would result in an M_w 6.6–6.8 event, manifesting the surface slip missing in the 2010 Léogâne earthquake. If such a rupture were to propagate to neighbouring sections of the EGPF to the west and east that did not slip in 2010, including the fault directly adjacent to Port-au-Prince, an earthquake larger than the 2010 event is certainly possible.

Information from the seismic wavefield also helps to discriminate the order of rupture of the dominant faults in our favoured kinematic inversion (the EPGF-like structure and the Léogâne fault, A and B in Fig. 3 and the following text). The first-motion focal mechanism for this earthquake (Supplementary Fig. S12) indicates that left-lateral strike-slip motion preceded any thrust motion; the presence of dilatational observations to the north and northwest of the epicentre cannot be matched by a thrust mechanism with a 55° dip to the north. From a Coulomb-stress-transfer perspective, this scenario is less favourable than the opposite (Supplementary Fig. S6c), in which slip on fault B triggers motion on fault A, unclamping the deep section of fault A to slip with left-lateral motion, and

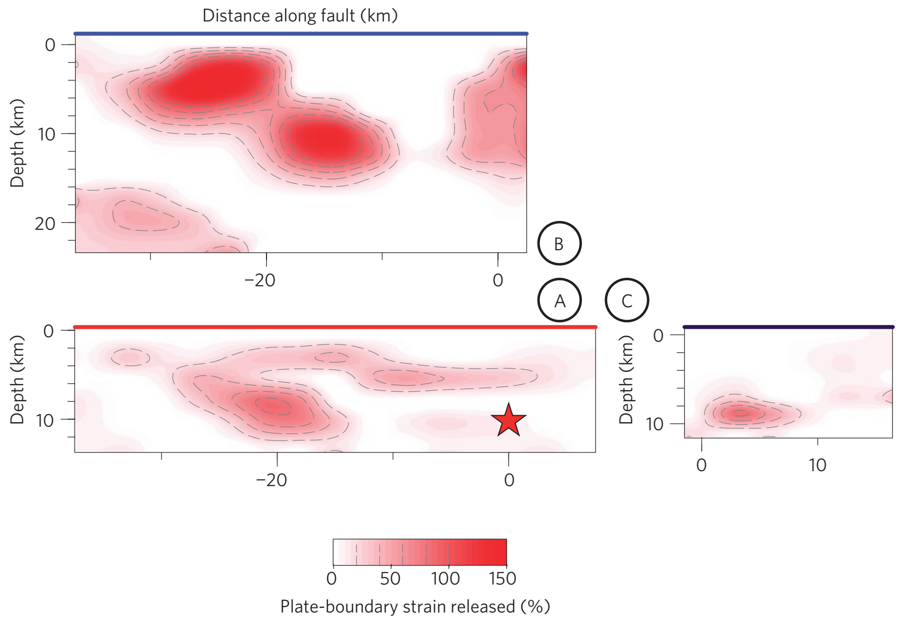

Figure 4 | Plate-boundary moment release. Cross-sectional projections of the amount of horizontal plate-boundary moment released during the 2010 Léogâne earthquake, as a percentage of the moment accumulated since 1770, based on our preferred rupture model for the earthquake. Fault planes A, B and C correlate to the steeply south-dipping EPGF fault trace, the more shallowly north-dipping fault most dominant in the earthquake rupture and the eastern, south-dipping 45° thrust structure, respectively (also shown in Fig. 3).

clamping its shallow section where we observe no surface rupture. The lack of positive Coulomb-stress changes imposed by left-lateral slip on fault A, and resolved onto the blind thrust fault B (Supplementary Fig. S6a,b) argue that, over the short timescale of this rupture, dynamic stresses play the driving role in rupture propagation over the ∼10 km from the EPGF-like structure to the Léogâne fault.

The complexity of this event invites comparison with other global transpressional earthquakes whose rupture processes include simultaneous or near-simultaneous motion on strike-slip and thrust structures. These types of event include the 1957 Gobi-Altay, Mongolia, earthquake[13] (M 8.1), the 1988 Spitak, Armenia, earthquake[14] (M_w 7.8), the 1989 Loma Prieta, California, earthquake[15] (M_w 6.9), the 1997 Zirkuh, Iran, earthquake[16] (M_w 7.2), the 2002 Denali, Alaska, earthquake[17] (M_w 7.9), the 2003 Bam, Iran, earthquake[18] (M_w 6.6) and the 2008 Wenchuan, China, earthquake[19] (M_w 7.9). The relatively common occurrence of these types of event and the large amounts of damage many have caused suggest that such complexity is not uncommon, despite being difficult to incorporate into hazard analyses. This issue is particularly relevant to southern California, where thrust faults of the Transverse Ranges parallel and abut the San Andreas fault, and may rupture simultaneously with, be triggered by or trigger slip on the San Andreas in a major earthquake[20]. Given that the Haiti earthquake joins a long list of complex ruptures in transpressional regimes, future models of earthquake hazards in similar settings might do well to regard multifault and blind ruptures as typical, rather than unusual.

The 2010 Léogâne earthquake will not leave a clear geological record that will be easily recognized by standard paleoseismic techniques because surface deformation was broadly distributed and surface rupture did not occur on the primary plate-boundary structure. Slip during this event caused uplift in areas of clear long-term subsidence while depressing high topography, implying that this type of event is either atypical, or indicates a modern reorganization of the fault system. Off-fault records of earthquake recurrence, such as multiple upraised dissolution or bioerosion notches along the coast (Supplementary Fig. S3) or evaluation of liquefaction features, may reveal a recurrence history for 2010-type events. Indirect palaeoseismic techniques like this are not usually applied to major, through-going strike-slip systems such as the EPGF, but they may reveal evidence of previously unrecognized, large earthquakes caused by off-fault deformation in similar tectonic settings.

Methods

We model the earthquake source as a rupture front of finite width propagating on two-dimensional planar fault segments[21]. We use a simulated-annealing algorithm to search for the combinations of slip amplitude, rake angle, rupture velocity and rise-time at each subfault element that best explains the teleseismic records, uplift observations and InSAR images of the event[22]. To improve the robustness and the efficiency of this optimization problem, the seismic data are decomposed in the wavelet domain, and the error function is defined as a combination of an L1 and an L2 norm. We also apply a Laplacian smoothing operator to reduce the dimensions of the parameter, thereby compensating for limitations in the data. For each inverted fault plane, the rake angle is constrained to be between 0° and 60° (global centroid moment tensor rake ±30°) on the steep south-dipping fault segment, and between 0° and 90° (increased to enable thrust motion) on the shallower north- and south-dipping fault segments. The rupture velocity is allowed to vary between 2.8 and 3.2 km s^{-1}. The shallowest cells on each fault plane are constrained to have zero slip to match the observed lack of surface rupture. The teleseismic dataset is made up of 21 P and 16 SH broadband waveforms, bandpass filtered from 2 s to 100 s, selected from the Global Seismographic Network on the basis of the quality of their signal-to-noise ratios and their contributions to even azimuthal coverage. Details of the InSAR data, inversion methods and field studies are given in Supplementary Information.

Received 24 May 2010; accepted 9 September 2010; published online 10 October 2010

References

1. Cavallo, E., Powell, A. & Becerra, O. *Estimating the Direct Economic Damage of the Earthquake in Haiti* (RES Working Papers 4652, Inter-American Development Bank, Research Department, 2010).
2. Dixon, T. *et al.* Relative motion between the Caribbean and North American plates and related boundary zone deformation based on a decade of GPS observations. *J. Geophys. Res.* **103,** 15157–15182 (1998).
3. Manaker, D. M. *et al.* Interseismic plate coupling and strain partitioning in the Northeastern Caribbean. *Geophys. J. Int.* **174,** 889–903 (2008).
4. Mann, P. *et al. 18th Caribbean Geological Conference, March 24–28, 2008, Santo Domingo* http://www.ig.utexas.edu/jsg/18_cgg/Mann3.htm.

5. Mann, P., Matumoto, T. & Burke, K. Neotectonics of Hispaniola—plate motion, sedimentation, and seismicity at a restraining bend. *Earth Planet. Sci. Lett.* **70,** 311–324 (1984).
6. Frohlich, C. & Apperson, K. D. Earthquake focal mechanisms, moment tensors, and the consistency of seismic activity near plate boundaries. *Tectonics* **11,** 279–296 (1992).
7. Prentice, C. S. *et al.* Seismic hazard of the Enriquillo Plantain Garden fault in Haiti inferred from palaeoseismology. *Nature Geosci.* doi:10.1038/ngeo991 (in the press).
8. Nettles, M. & Hjörleifsdóttir, V. Earthquake source parameters for the January 12 Haiti main shock and aftershock sequence. *Geophys. J. Int.* **183,** 375–380 (2010).
9. Taylor, F. W., Frohlich, C., Lecolle, J. & Strecker, M. Analysis of partially emerged coals and reef terraces in the central Vanuatu arc: Comparison of contemporary coseismic and nonseismic with quaternary vertical movements. *J. Geophys. Res.* **92,** 4905–4933 (1987).
10. Briggs, R. W. *et al.* Deformation and slip along the Sunda megathrust in the great 2005 Nias–Simeulue earthquake. *Science* **311,** 1897–1901 (2006).
11. Calais, E. *et al.* Transpressional rupture of an unmapped fault during the 2010 Haiti earthquake. *Nature Geosci.* doi:10.1038/ngeo992 (in the press).
12. Puebellier, M., Mauffret, A., Leroy, S., Vlia, J. M. & Amilcar, H. Plate boundary readjustment in oblique convergence: Example of the Neogene of Hispaniola, Greater Antilles. *Tectonics* **19,** 630–648 (2000).
13. Florensov, N. A. & Solonenko, V. P. (eds) *The Gobi-Altai Earthquake* (Akademiya Nauk USSR, 1963) [in Russian] (English translation, US Department of Commerce, 1965).
14. Pacheco, J. F., Estabrook, C. H., Simpson, D. W. & Nábêlek, J.L. Teleseismic body wave analysis of the 1988 Armenian earthquake. *Geophys. Res. Lett.* **16,** 1425–1428 (1989).
15. Hanks, T. C. & Krawinkler, H. The 1989 Loma Prieta earthquake and its effects: Introduction to the special issue. *Bull. Seismol. Soc. Am.* **81,** 1415–1423 (1991).
16. Berberian, M. *et al.* The 1997 May 10 Zirkuh (Qa'enat) earthquake (M_w 7.2): Faulting along the Sistan suture zone of eastern Iran. *Geophys. Res. Lett.* **136,** 671–694 (1999).
17. Aagaard, B. T., Anderson, G. & Hudnut, K. W. Dynamic rupture modeling of the transition from thrust to strike-slip motion in the 2002 Denali fault earthquake, Alaska. *Bull. Seismol. Soc. Am.* **94,** S190–S201 (2004).
18. Talebian, M. *et al.* The 2003 Bam (Iran) earthquake: Rupture of a blind strike-slip fault. *Geophys. Res. Lett.* **31,** L11611 (2004).
19. Liu-Zeng, J. *et al.* Co-seismic ruptures of the 12 May 2008, Ms 8.0 Wenchuan earthquake, Sichuan: East–west crustal shortening on oblique, parallel thrusts along the eastern edge of Tibet. *Earth Planet. Sci. Lett.* **286,** 355–270 (2009).
20. Bayarsayhan, C. *et al.* 1957 Gobi-Altay, Mongolia, earthquake as a prototype for southern California's most devastating earthquake. *Geology* **24,** 579–582 (1996).
21. Heaton, T. H. Evidence for and implications of self-healing pulses of slip in earthquake rupture. *Phys. Earth Planet. Inter.* **64,** 1–20 (1990).
22. Ji, C., Helmberger, D. V. & Wald, D. J. A teleseismic study of the 2002, Denali, Alaska, earthquake and implications for rapid strong motion estimation. *Earthq. Spectra* **20,** 617–637 (2004).
23. Wessel, P. & Smith, W. H. F. New, improved version of Generic Mapping Tools released. *EOS Trans. AGU* **79,** 579 (1998).

Acknowledgements

We thank V. Tsai, H. Benz, J. McCarthy, R. Bilham and three anonymous reviewers for their comments in improving this manuscript. The study benefited greatly from the assistance of P. Jean of Le Bureau des Mines et de l'Energie d'Haiti, and from the logistical aid of R. Boyer. We thank K. Ludwig and J. Kindinger of USGS and the captain and crew of the RV *Endeavor* for use and transport of the rigid-hulled inflatable boat. We thank G. Choy for the first-motion focal mechanism. We thank R. Bilham and R. Koehler for early field observations of coastal deformation. Fieldwork studies were sponsored by the US Agency for International Development, USGS and the National Science Foundation. PALSAR level 1.0 data are shared among PIXEL (PALSAR Interferometry Consortium to Study our Evolving Land Surface), and provided from the Japanese Aerospace Exploration Agency under a cooperative research contract with the Earthquake Research Institute, University of Tokyo. Early PALSAR data were provided under the Group on Earth Observation Geohazards Supersite programme and other scenes through the Alaska Satellite Facility. The ownership of PALSAR data belongs to METI (Ministry of Economy, Trade and Industry) and the Japanese Aerospace Exploration Agency. G.P.H. is contracted to work for the USGS by Synergetics Inc., Fort Collins, Colorado. A.S. and M.S. are partially supported under funds provided by the Gordon and Betty Moore Foundation through the Tectonics Observatory. This paper is Caltech Tectonic Observatory contribution 138. Part of the research described in this publication was carried out at the Jet Propulsion Laboratory, California Institute of Technology, under contract with the National Aeronautics and Space Administration. Figures have been made using the Generic Mapping Tools of Wessel and Smith[23]. Fieldwork partially supported by NSF-EAR RAPID grant 1024990. UTIG contribution no. 2285.

Author contributions

G.P.H. and R.W.B. were responsible for writing the main manuscript and supplement and generating figures. G.P.H. conducted seismic fault inversions and moment-balance calculations. E.J.F. carried out InSAR analysis. G.P.H., R.W.B., A.S. and E.J.F. were jointly responsible for the fault model. A.S. carried out joint inversions in collaboration with E.J.F., M.S. and T.I. R.W.B., C.P., K.H., P.M., F.W.T., A.J.C. and R.G. were all involved in field studies and contributed data and interpretations from these studies. PALSAR data were provided to T.I. under the JAXA cooperative agreement. All authors contributed to the interpretation of results and discussion of ideas in this study.

Additional information

The authors declare no competing financial interests. Supplementary information accompanies this paper on www.nature.com/naturegeoscience. Reprints and permissions information is available online at http://npg.nature.com/reprintsandpermissions. Correspondence and requests for materials should be addressed to G.P.H.